

# Angular clustering of point sources at 150 MHz in the TGSS survey

Sandeep Rana<sup>\*</sup>, Jasjeet S. Bagla<sup>†</sup>

*Indian Institute of Science Education and Research Mohali, Knowledge City, Sector 81, Sahibzada Ajit Singh Nagar, Punjab 140306, India*

15 September 2022

## ABSTRACT

We study the angular clustering of point sources in The GMRT Sky Survey (TGSS). The survey at 150 MHz with  $\delta > -53.5^\circ$  has a sky coverage of  $3.6\pi$  steradian, i.e., 90% of the whole sky. We define our sample and study angular clustering of point sources at large scales for different subsamples. We find that there is a break in angular clustering at a scale of about one degree. We compare our results with other studies of clustering of point sources. We use the available data to present the variation of clustering with the flux limit at 150 MHz. We also present results of cross-matching sources with the SDSS redshift surveys and estimation of the two point correlation function.

**Key words:** Cosmology: large-scale structure of Universe, observation, miscellaneous radio continuum: general

## 1 INTRODUCTION

Low frequency observations of radio sources give unique information about the population of ultra-relativistic electrons in the inter-stellar medium (ISM) of galaxies: synchrotron emission is the primary radiative mechanism at these frequencies (Condon 1992). However, emission from ISM in galaxies and AGNs dominates over the expected flux from neutral Hydrogen via the redshifted 21 cm radiation from the early universe. This then constitutes a significant foreground that needs to be studied and removed in order to study the evolution of neutral Hydrogen in the universe. In particular this affects studies of the so called epoch of reionization (EoR) where the inter-galactic medium transitions from being neutral to almost completely ionised (Di Matteo et al. 2004; Liu et al. 2009; Jélic et al. 2008; Trott et al. 2012; Murray et al. 2017; Spinelli, Bernardi, & Santos 2018). Redshifted 21 cm radiation from this epoch is likely to have observed wavelength of 1.5–4 m, or frequency of 75–200 MHz. Therefore a study of point sources and their clustering in this range of frequencies is relevant, not just from the perspective of studying radio populations but also for its impact on EoR studies. Studies of radio source clustering beyond angular correlation function require information about redshift, which is not available for an overwhelming majority of sources at present.

A number of studies have been carried out to quantify the faint source population and its clustering at low frequen-

cies. A list of existing and ongoing radio surveys is given in Table 1.

The Giant Metrewave Radio Telescope (GMRT) was used to survey the Radio Sky at 150 MHz between 2010 and 2012<sup>1</sup>. Alternative Data Release (ADR1) (Intema et al. 2017) of the TGSS survey contains a catalogue of point sources. Here, TGSS data has been analysed using the SPAM pipeline, which includes corrections for direction-dependent ionospheric phase effects. Also included are continuum Stokes I images of 99.5% of the radio sky north of  $\delta = -53^\circ$  ( $3.6\pi$  sr, or 90% of the full sky) at a resolution of  $25'' \times 25''$  north of  $\delta = 19^\circ$  and  $25'' \times 25'' / \cos(\delta - 19^\circ)$  south of  $\delta = 19^\circ$ , and a median noise of  $3.5 \text{ mJy beam}^{-1}$ . The extracted radio source catalogue contains positions, flux densities, sizes and more for 0.62 Million sources down to a  $7\sigma$  peak-to-noise threshold<sup>2</sup>. The data analysis pipeline and data products are described in detail in Intema et al. (2017).

The median survey sensitivity is  $3.5 \text{ mJy beam}^{-1}$  and most part of sky (about 80%) covered by TGSS has sensitivity  $5 \text{ mJy beam}^{-1}$  (see figure 8 of Intema et al. (2017)). The estimation of the TGSS confusion noise at 150 MHz and with a  $25''$  beam ranges between  $0.44 \text{ mJy beam}^{-1}$  and  $2.5 \text{ mJy beam}^{-1}$  in most of the sky. The TGSS point source survey has 50 percent completeness at  $25 \text{ mJy}$  (or  $7\sigma$  for point sources, with sigma being the median survey noise of  $3.5 \text{ mJy beam}^{-1}$ ) for more detail see Intema et al. (2017).

<sup>1</sup> Proposal for the survey was made by Sandeep Sirothia, Nimisha Kantharia, Ishwara Chandra and Gopal Krishna (GTAC Cycle 18).

<sup>2</sup> <http://tgssadr.strw.leidenuniv.nl/doku.php>

<sup>\*</sup> E-Mail: sandeep@iisermohali.ac.in

<sup>†</sup> E-Mail: jasjeet@iisermohali.ac.in

**Table 1.** Low frequency sky surveys. This table enumerates various sky surveys at low frequencies. Their sky coverage and sensitivity, frequency and resolution are listed here.

Survey	Frequency(MHz)	Resolution	Noise (mJy beam <sup>-1</sup> )
VLSS(Cohen et al. (2007))	74	80''	100
VLSSr(Lane et al. (2014))	73.8	75''	100
8C(Rees (1990))	38	4.5' × 4.5' csc(δ)	200 – 300
7C(Pooley et al. (1998))	151	70'' × 70'' csc(δ)	20
MSSS-LBA(Heald et al. (2015))	30 – 78	≤ 150''	≤ 50
MSSS-HBA(Heald et al. (2015))	120 – 170	≤ 120''	≤ 10 – 15
TGSS Intema et al. (2017)	150	25''	5
GLEAM(Hurley-Walker et al. (2017))	72 – 231	100''	10
LoTTS(Shimwell et al. (2017))	120 – 168	25''	0.5

We choose to work with subsets with higher flux cutoff to ensure better completeness.

## 2 ANALYSIS AND RESULTS

### 2.1 Survey Selection

Our main aim here is to do study clustering of point sources. We need to define a sample that is homogeneous and complete. The ADR1 data provides us with peak flux, source flux and noise on the individual source. We created a pixelised all-sky map for all sources in TGSS ADR1 catalogue with  $N_{side} = 128$  and 1024 using HEALPy: python version for HEALPix. We then masked all pixels with noise level of  $> 4$  mJy beam<sup>-1</sup> using a binary mask. The resulting map is shown in figure 1.

We used an  $N_{side} = 1024$  map as selection function to generate random catalogues. For radio sources, we used the same noise map with an additional cut on source peak flux which is  $> 32$  mJy beam<sup>-1</sup> as shown in figure 2, taking this as selection map for source catalogue, we created different source population subsets using total source flux of  $\geq 50$  mJy, 60 mJy, 100 mJy and 200 mJy. The total number of source for flux of  $\geq 50$  mJy, 60 mJy, 100 mJy and 200 mJy are 307634, 275780, 188269, 100985 respectively. Each of the subsets is fairly large for a robust clustering analysis at 150 MHz.

Note that  $S \geq 60$  mJy at 150 MHz corresponds to NVSS  $S \geq 10$  mJy, this correspondence is computed using a typical spectral index relation (Tiwari 2016; Intema et al. 2017):

$$\alpha_{obs} = \frac{(\log S_{TGSS} - \log S_{NVSS})}{(\log \nu_{NVSS} - \log \nu_{TGSS})} \quad (1)$$

Where  $\nu_{NVSS} = 1.4$  GHz,  $\nu_{TGSS} = 150$  MHz and  $S_{TGSS}$  and  $S_{NVSS}$  are, respectively, the flux densities measured by the TGSS and NVSS for sources common to the two catalogues. We used  $\alpha_{obs} = 0.76$  for conversion, see figure 2 of Tiwari (2016) for details.

### 2.2 Angular Correlation Function

The angular correlation function  $\omega(\theta)$  describes the clustering of sources on the sky. We calculate  $\omega(\theta)$  using the Landy-Szalay estimator (Landy & Szalay 1993) as it is known to be

the most robust estimator and it takes care of edge corrections (Kerscher et al. 2000). The angular correlation function is defined in terms of pair counts in the data and the random catalog:

$$\omega(\theta) = \frac{N_r(N_r + 1)DD}{N_d(N_d + 1)RR} - N_d(N_r + 1)\frac{DR}{RR} + 1 \quad (2)$$

Here DD denotes the count of pairs in the data at angular separation  $\theta$ , and  $N_d$  denotes the total number of objects considered in the analysis. Similarly, RR is the averaged pair count over a catalogue of uniformly distributed points covering the same survey area, DR is the data-random cross pair count, and  $N_r$  denotes the number of points in the random catalogue. We created  $10^3$  random catalogs for clustering analysis using survey selection function as described in previous section.

To compute DD, RR and DR efficiently we use publicly available routines such as KD-tree and BD-tree (Scikit-learn (Pedregosa et al. 2011)) which are an implementation of spatial algorithm such as k-d tree and Ball tree data structures for fast nearest neighbour search (Bentley 1975; Omohundro 1989). We used bootstrap re-sampling method for error estimation in angular correlation (Feigelson & Babu 2012; Andrae 2010).

We find that the amplitude of the angular correlation function varies monotonically with the flux cut-off at all scales, as shown in figure 2. We find that as the flux threshold is increased, the amplitude of angular correlation function at a fixed angle increases.

To quantify the shape of the angular correlation function, we assume a power law form:  $A\theta^{-\gamma}$  (Cress et al. 1996; Rengelink 1999; Magliocchetti et al. 1998; Blake & Wall 2002; Overzier et al. 2003; Blake et al. 2004). This is used to fit data at angular scales larger than a degree. Here  $A$  is the amplitude,  $\theta$  is the angle in degrees and  $\gamma$  is the power law index. We estimate the posterior probability distribution alongside best fit for amplitude  $A$  and power law index  $\gamma$ . We use the *emcee* (Foreman-Mackey et al. 2013) package, which is a Python implementation of MCMC sampling for this estimation.

Figure 3 shows the  $1 - \sigma$  and  $2 - \sigma$  confidence interval for the subsamples with different flux cut-off. These are plotted in the  $A - \gamma$  plane and we see that as the flux cut-off increases, the dominant effect is an increase in  $A$ . The preferred range for  $\gamma$  does not show any strong evolution ex-

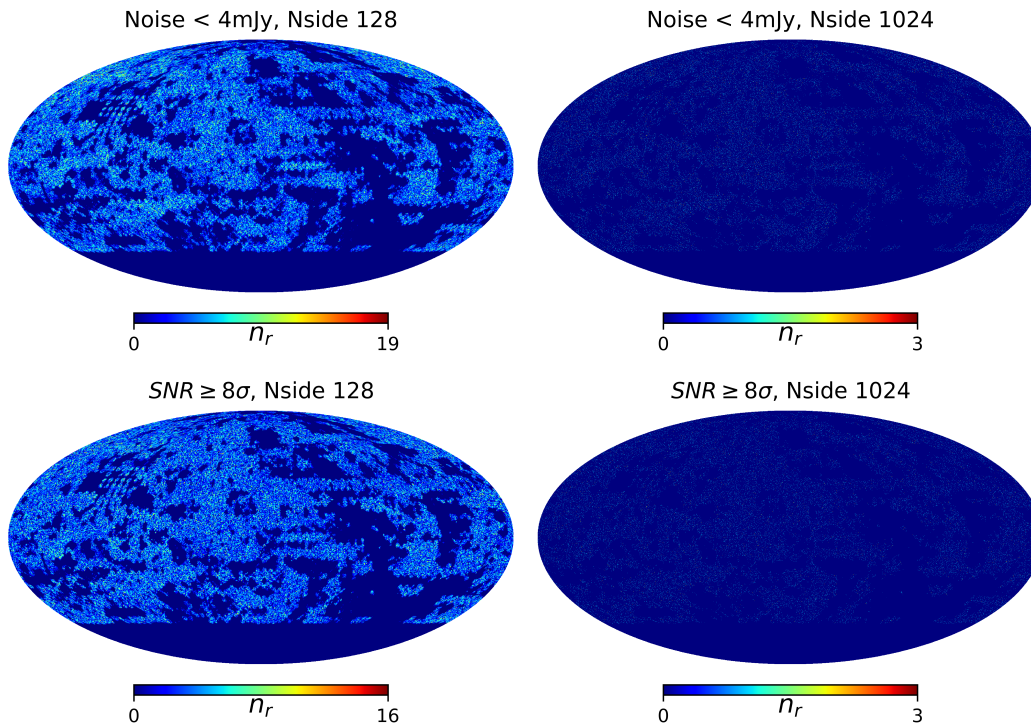


**Figure 1.** Number density of sources with noise  $\leq 4$  mJy/beam with  $N_{\text{side}} = 128$  and 1024, we use this as our angular selection function for our correlation analysis. Number density of sources with  $\text{SNR} \geq 8$  for  $N_{\text{side}} = 128$  and 1024: We use this as our main population for our correlation analysis.

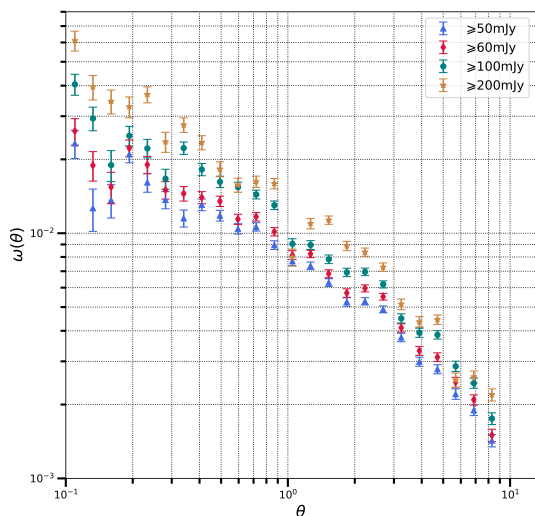


**Figure 2.** Angular correlation function for the four subsets. We see that there is a break in the shape at an angle of  $1^\circ$  with a power law decline at larger scales and a gentler variation at smaller scales. The amplitude of angular correlation is larger for subsamples with a high flux threshold, i.e., brighter sources cluster more strongly.

cept for the highest cut-off of 200 mJy. Here, we see that the angular correlation function has a strongly enhanced amplitude  $A$  and also a steeper slope  $\gamma$ .

In table 2 we have enumerated clustering studies of radio sources in surveys carried out at different frequencies (de Oliveira-Costa & Lazio 2010). We find that if we consider surveys with a comparable flux cut-off, as determined by the average spectral index. This is illustrated in figure 4. This figure shows the variation of the amplitude of angular clustering as a function of the scaled flux threshold in different samples. The scaling here has been done assuming a spectral index 0.76. We find that there is a clear trend where increasing the scaled flux threshold leads to a higher amplitude for the amplitude of clustering. However, we see some scatter around this trend, unlike figure 1 of (Rengelink 1999). The source of scatter is unclear and it may be due to sample variance or variations in spectral index that leads to a bias.

The line plotted in the top panel of figure 4 is the best fit power law for these data points of the form  $a \times 10^{-3} (S_{\text{min}} / (1 \text{ mJy}))^b$ . Note that the fit is driven by points with smaller error, as expected. The lower panel shows the confidence levels of the power law fit. Note that there is no significant variation in the index  $\gamma$  of the angular correlation function with flux limit in our sample at lower flux levels. Thus the fitted variation of the amplitude of angular clustering can be used for simulations of point source foregrounds at and around 150 MHz. Indeed, this allows for an approach that is independent of the modelling of different types of

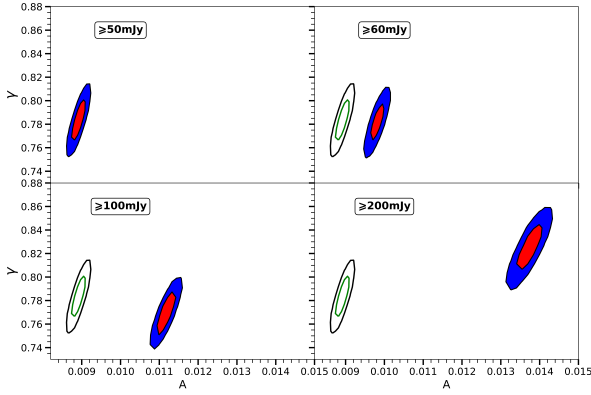


**Figure 3.** Posterior probability distribution for  $A$  and  $\gamma$  using angular correlation data for different flux cut-off values. This is shown for the four subsets.  $1 - \sigma$  and  $2 - \sigma$  contours are shown here. The outline of contours for the 50 mJy subset is shown in all the panels for reference.

radio sources (Di Matteo et al. 2004; Jélic et al. 2008; Liu et al. 2009; Trott et al. 2012; Murray et al. 2017).

### 2.3 Spatial clustering of radio sources

Angular correlation function of a set of sources can be combined with the knowledge of the redshift distribution of sources to estimate the two point correlation function of these sources in three dimensional space (Limber 1954; Efstathiou et al. 1991; Baugh & Efstathiou 1993; Loan et al. 1997; Magliocchetti et al. 1998; Simon 2007). In order to get an estimate of the redshift distribution, we cross match TGSS sources with the SDSS data. Spectroscopic as well as photometric redshifts have been used here and results are marked to indicate the set used. Cross matches within a search radius of  $5''$  for the TGSS and SDSS catalogues were used. We chose this search radius as we expect locations of sources to be much better known than the resolution<sup>3</sup>. The number of such cross matches is very small, i.e., 829 sources with spectroscopic redshift for search radius of  $5''$  corresponds to flux cut-off of  $\geq 50$  mJy and 1706 with photometric redshift hence the redshift distribution of a vast majority of sources remains uncertain. For reference, we note that these cross matched sources are less than 0.3% and 0.6% of the 50 mJy catalogue, respectively. Hence results presented here should be thought of as first estimates. The redshift distribution of cross matches for the two catalogue is shown in figure 5. We analyse the properties of galaxies with cross-matches and find that most of these are bright red galaxies (see figure 7 and discussion below.).

In general, we need to take the evolution of the correlation function with epoch into account. This is certainly important when the sources are distributed out to high redshifts. The highest redshift cross match we have here is

<sup>3</sup> Huib Intema (Leiden) intema@strw.leidenuniv.nl, private communication

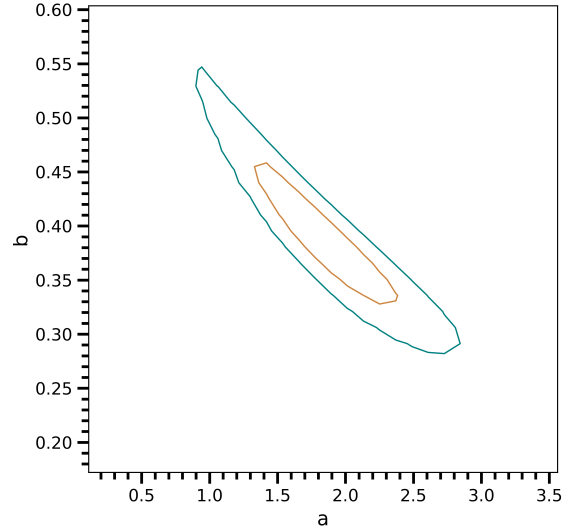
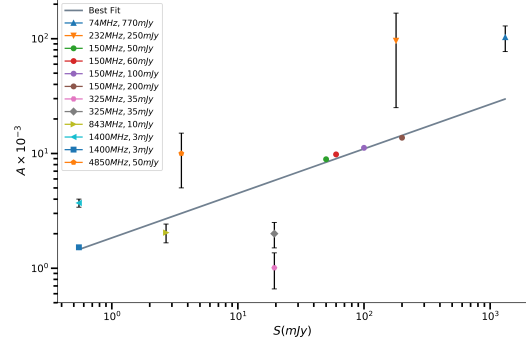


**Figure 4.** We show the amplitude of correlation function as a function of the scaled flux threshold from different studies. See text for details of the scaling procedure. We find a trend of a higher correlation amplitude for a higher flux threshold. The error bars on points from some of the studies, including the present work, are too small to be depicted. The line plotted in the top panel is the best fit power law for these data points of the form  $a \times 10^{-3} (S_{min}/(1 \text{ mJy}))^b$ . The lower panel shows the confidence level intervals of the power law fit in the amplitude ( $a$ ) and index ( $b$ ) space.

$z \sim 0.34$  for spectroscopic data and  $z \sim 0.92$  for photometric data set, although the bulk of the cross matches are at much lower redshifts.

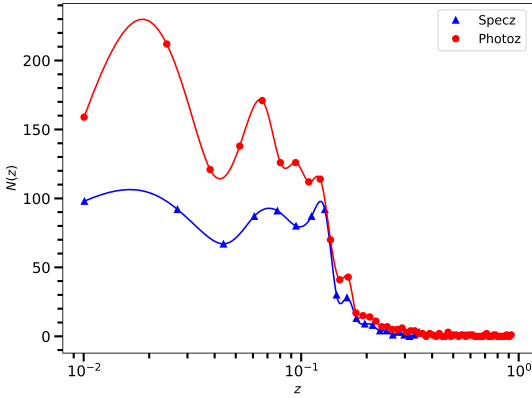
We assume a redshift-dependent power law form for spatial correlation function for our analysis.

$$\xi(r, z) = \left(\frac{r_0}{r}\right)^{\gamma_r} (1+z)^{-(3+\epsilon-\gamma_r)} \quad (3)$$

Where  $\epsilon = \gamma_r - 3$  corresponds to stable clustering in co-moving coordinates,  $\epsilon = 0$  is for stable clustering in proper coordinates and  $\epsilon = \gamma_r - 1$  is for clustering growth in linear regime (Efstathiou et al. 1991; Loan et al. 1997). For small angles ( $\theta \ll 1$  rad) the angular correlation  $\omega(\theta)$  can be related to the two point correlation function  $\xi(r, z)$  if we

**Table 2.** Best fit value of  $\omega(\theta)$  at low frequencies from current study and earlier published work.

Ref	$\nu$ (MHz)	$S_{lim}(mJy)$	$A (\times 10^{-3})$	$\gamma$	SourcesNumber
This Work	150	$\geq 50$	$8.9 \pm 0.2$	$0.7832 \pm 0.0176$	307634
This Work	150	$\geq 60$	$9.8 \pm 0.2$	$0.7818 \pm 0.0172$	275780
This Work	150	$\geq 100$	$11.2 \pm 0.2$	$0.7700 \pm 0.0182$	188269
This Work	150	$\geq 200$	$13.7 \pm 0.3$	$0.8246 \pm 0.0210$	100985
de Oliveira-Costa & Capodilupo (2010)	74	770	$103 \pm 26$	$1.21 \pm 0.35$	68311
de Oliveira-Costa & Lazio (2010)	232	250	$96 \pm 71$	$1.12 \pm 0.11$	34426
Loan et al. (1997)	$4.85 \times 10^3$	50	$10.0 \pm 5.0$	1.8	77856
Cress et al. (1996)	1400	3	$3.7 \pm 0.3$	$1.06 \pm 0.03$	109873
Magliocchetti et al. (1998)	1400	3	$1.52 \pm 0.06$	$1.68 \pm 0.07$	86074
Rengelink (1999)	325	35	$2.0 \pm 0.5$	0.8	86461
Blake et al. (2004)	325	35	$1.01 \pm 0.35$	$1.22 \pm 0.33$	86461
Blake et al. (2004)	843	10	$2.04 \pm 0.38$	$1.24 \pm 0.16$	68373


**Figure 5.** Redshift distribution of cross-matched SDSS galaxies within search radius  $5''$  for flux cut-off  $\geq 50$  mJy. We note that bulk of the cross matches are at  $z < 0.15$ .

assume the form given above (Efstathiou et al. 1991):

$$w(\theta) = \sqrt{\pi} \frac{\Gamma[(\gamma_r - 1)/2]}{\Gamma(\gamma_r/2)} A r_0^{\gamma_r} \theta^{1-\gamma_r} \quad (4)$$

where

$$A = \frac{\int_0^\infty \left(\frac{dz}{dx}\right) x^{1-\gamma_r} F(x) (1+z)^{-(3+\epsilon-\gamma_r)} \left(\frac{dN}{dz}\right)^2 dz}{\left[\int_0^\infty \left(\frac{dN}{dz}\right) dz\right]^2} \quad (5)$$

Here  $x$  is the comoving distance at redshift  $z$  and  $dN/dz$  is the number of the object per unit redshift of TGSS galaxies.

We use this relation to constrain the values of  $r_0$  and  $\gamma_r$  for different values of  $\epsilon$ . We do not take the different variation of  $w(\theta)$  at smaller angles into account as it pertains to very small length scales in the context of the cross-matched sample:  $\theta = 1^\circ$  corresponds to a length scale smaller than 1 Mpc at  $z \sim 0.1$  and most of the cross-matches are at lower redshift. The results obtained from the analysis are shown in Figure 6 showing best fit value and  $1-\sigma$  and  $2-\sigma$  confidence interval for 50 mJy flux cut-off. We find that there is some

**Table 3.** Best fit parameters describing the two point correlation function for the Spectroscopic and Photometric cross-matched redshift distributions. The first three rows give the numbers for the redshift distribution derived from cross matching of TGSS sources with the spectroscopic galaxy redshift catalogue. The next (and last) three rows give the same for redshift distribution derived from cross matching of TGSS sources with the photometric redshift catalogue. All results presented here are for a flux cut-off of 50 mJy.

$r_0(h^{-1} \text{ Mpc})$	$\gamma_r$	$\epsilon$
$11.051 \pm 0.720$	$1.784 \pm 0.0175$	0
$11.565 \pm 0.771$	$1.784 \pm 0.01767$	$\gamma_r - 1$
$10.306 \pm 0.697$	$1.784 \pm 0.0178$	$\gamma_r - 3$
$11.679 \pm 0.859$	$1.784 \pm 0.0176$	0
$11.891 \pm 0.879$	$1.784 \pm 0.0177$	$\gamma_r - 1$
$11.314 \pm 0.847$	$1.784 \pm 0.0177$	$\gamma_r - 3$

degeneracy between the two parameters from the elongated ellipsoid. We do not see any strong variation with the choice of  $\epsilon$ . This is to be expected as the redshift distribution of sources with cross matches is limited to low redshifts. Table 3 provides a summary of these results for the two cross-matched catalogues. In each case we find that the slope and the amplitude of the correlation function is consistent with correlation of bright red galaxies (Zehavi et al. 2011).

To explore this further we plot  $u-r$  colour vs  $r$ -band absolute magnitude for our sample see figure 7 we used  $u-r$  cut given by Strateva et al. (2001). One can clearly see that bulk of our sample is dominated by red early type galaxies. This is true of both the spectroscopic and photometric redshift sample cross-matches. Thus the slope and amplitude of the correlation function is consistent with the type of galaxies with cross-matches. However, the number of cross-matches are so few that it is difficult to deduce the two point correlation function for the full sample.

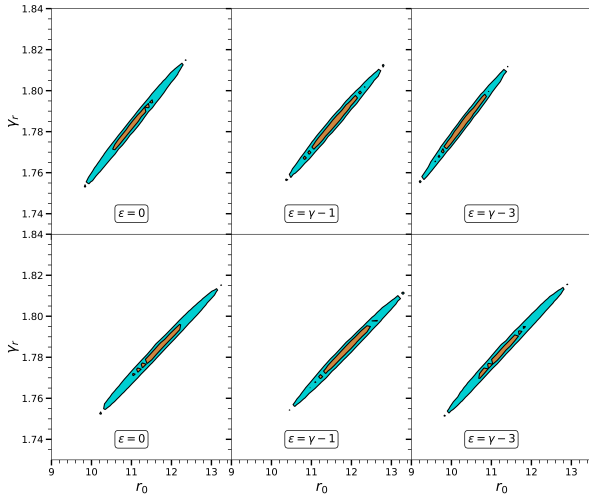


**Figure 6.** Posterior probability distribution for  $r_0$  and  $\gamma_r$  for flux cut-off of  $\geq 50$  mJy. Upper panel is for spectroscopic redshift data corresponds to  $\geq 50$  mJy flux cut-off and  $5''$  cross-matching radius. Similarly lower panel is for photometric redshift data.

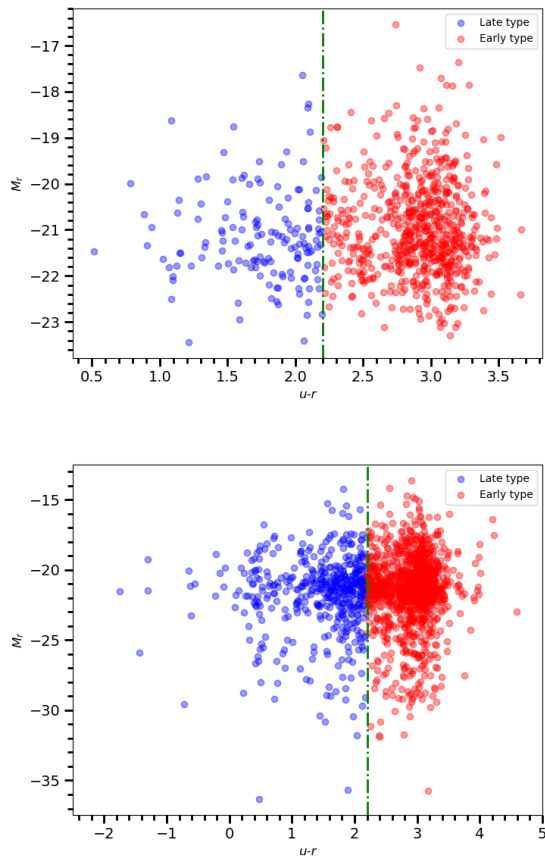


**Figure 7.**  $u - r$  vs  $r$ -band absolute magnitude, top panel is for the spectroscopic sample and bottom one is for the photometric sample.  $u - r = 2.2$  divides the red galaxies from blue (Strateva et al. 2001).

### 3 SUMMARY

In this paper we have studied angular clustering of radio sourced in the TGSS survey using the catalogues derived in the alternative data release. We have defined our main sample and sub samples using the rms noise and peak flux. We have studied angular clustering of these sources and our main findings are:

- (i) The angular correlation function has a power law behaviour at scales larger than a degree: correlation drops rapidly at larger angular separations.
- (ii) For most subsets the angular correlation at scales smaller than a degree has a weaker dependence on scale as compared to larger scales.
- (iii) The slope of the angular correlation function shows little variation with the flux of sources, except for the highest flux sub-sample with a lower cut-off of 200 mJy. In this case the angular correlation is steeper than for other sub-samples.
- (iv) The amplitude of the power law increases monotonically with the peak flux of sources.
- (v) We have compared our findings with other studies of angular clustering of radio sources. We show that assuming a typical spectral index of  $\alpha = 0.76$ , the amplitude of angular clustering is insensitive to the frequency at which the sources are observed and selected. This is in agreement with Rengelink (1999).

(vi) We provide a fit to the variation of the amplitude of clustering with the flux cutoff at 150 MHz. This is potentially useful for modelling of point source foregrounds for EoR studies.

We use cross matches with the SDSS spectroscopic and photometric samples and find some common sources. Using the redshift distribution of these sources we estimate the full two point correlation function of the TGSS sources. We find that the two point correlation function has an amplitude that is comparable with bright red galaxies. This is consistent with the galaxy population identified using cross-matches. However it does not enable us to make any statements about the two point correlation function for the full population as we have identified only a very small number of TGSS sources. For reasons not very clear, we are unable to find cross-matches for star forming galaxies, even though we understand that this is possible only at very low redshifts given the sensitivity of the TGSS (Schober, Schleicher, & Klessen 2017).

### ACKNOWLEDGEMENTS

The authors acknowledge the use of the HPC facility at IISER Mohali for this work. This research has made use of NASA's Astrophysics Data System Bibliographic Services.

### REFERENCES

- Andrae R., 2010, ArXiv e-prints  
 Baugh C., Efstathiou G., 1993, Monthly Notices of the Royal Astronomical Society, 265, 145  
 Bentley J. L., 1975, Commun. ACM, 18, 509  
 Blake C., Mauch T., Sadler E. M., 2004, MNRAS, 347, 787  
 Blake C., Wall J., 2002, MNRAS, 337, 993

- Cohen A. S., Lane W. M., Cotton W. D., Kassim N. E., Lazio T. J. W., Perley R. A., Condon J. J., Erickson W. C., 2007, *AJ*, 134, 1245
- Condon J. J., 1992, *ARA&A*, 30, 575
- Cress C. M., Helfand D. J., Becker R. H., Gregg M. D., White R. L., 1996, *ApJ*, 473, 7
- de Oliveira-Costa A., Capodilupo J., 2010, *MNRAS*, 404, 1962
- de Oliveira-Costa A., Lazio J., 2010, *ArXiv e-prints*
- Di Matteo T., Ciardi B., Miniati F., 2004, *Monthly Notices of the Royal Astronomical Society*, 355, 1053
- Efstathiou G., Bernstein G., Tyson J. A., Katz N., Guhathakurta P., 1991, *ApJ*, 380, L47
- Feigelson E. D., Babu G. J., 2012
- Foreman-Mackey D., Hogg D. W., Lang D., Goodman J., 2013, *PASP*, 125, 306
- Heald G. H., Pizzo R. F., Orrú E., Breton R. P., Carbone D., Ferrari C., Hardcastle M. J., 2015, *A&A*, 582, A123
- Hurley-Walker N., Callingham J. R., Hancock P. J., Franzen T. M. O., Hindson L., Kapińska A. D., Morgan J., Offringa A. R., Wayth R. B., Wu C., 2017, *MNRAS*, 464, 1146
- Intema H. T., Jagannathan P., Mooley K. P., Frail D. A., 2017, *A&A*, 598, A78
- Kerscher M., Szalay A. S., 2000, *The Astrophysical Journal Letters*, 535, L13
- Landy S. D., Szalay A. S., 1993, *ApJ*, 412, 64
- Lane W. M., Cotton W. D., van Velzen S., Clarke T. E., Kassim N. E., Helmboldt J. F., Lazio T. J. W., Cohen A. S., 2014, *MNRAS*, 440, 327
- Limber D. N., 1954, *ApJ*, 119, 655
- Liu A., Tegmark M., Zaldarriaga M., 2009, *MNRAS*, 394, 1575
- Loan A. J., Wall J. V., Lahav O., 1997, *MNRAS*, 286, 994
- Magliocchetti M., Maddox S. J., Lahav O., Wall J. V., 1998, *MNRAS*, 300, 257
- Murray S. G., Trott C. M., Jordan C. H., 2017, *The Astrophysical Journal*, 845, 7
- Omohundro S. M., 1989, *Technical report*, Five Balltree Construction Algorithms
- Overzier R. A., Röttgering H. J. A., Rengelink R. B., Wilman R. J., 2003, *A&A*, 405, 53
- Pedregosa F., Varoquaux G., Gramfort A., Michel V., Thirion B., Grisel O., Blondel M., Prettenhofer P., Weiss R., Dubourg V., Vanderplas J., Passos A., Cournapeau D., Brucher M., Perrot M., Duchesnay E., 2011, *Journal of Machine Learning Research*, 12, 2825
- Pooley D. M., Waldram E. M., Riley J. M., 1998, *Monthly Notices of the Royal Astronomical Society*, 298, 637
- Rees N., 1990, *MNRAS*, 244, 233
- Rengelink R., 1999, in Röttgering H. J. A., Best P. N., Lehnert M. D., eds, *The Most Distant Radio Galaxies Clustering evolution in the radio surveys WENSS and GB6*. p. 399
- Schober J., Schleicher D. R. G., Klessen R. S., 2017, *MNRAS*, 468, 946
- Shimwell T. W., Röttgering H. J. A., Best P. N., Williams W. L., Dijkema T. J., de Gasperin F., Hardcastle M. J., Heald G. H., 2017, *A&A*, 598, A104
- Simon P., 2007, *A&A*, 473, 711
- Spinelli M., Bernardi G., Santos M. G., 2018, *arXiv*, arXiv:1802.03060
- Tiwari P., 2016, *ArXiv* 1609.01308
- Trott C. M., Wayth R. B., Tingay S. J., 2012, *ApJ*, 757, 101
- Zehavi I., Zheng Z., Weinberg D. H., Blanton M. R., Bahcall N. A., Berlind A. A., Brinkmann J., Frieman J. A., Gunn J. E., Lupton R. H., Nichol R. C., Percival W. J., Schneider D. P., Skibba R. A., Strauss M. A., Tegmark M., York D. G., 2011, *ApJ*, 736, 59
- Jélic V., Zaroubi S., Labropoulos P., Thomas R. M., Bernardi G., Brentjens M. A., de Bruyn A. G., 2008, *MNRAS*, 389
- Strateva, I. and Ivezić, Ž. and Knapp, G. R. and Narayanan, V. K. and Strauss, M. A. and Gunn, J. E. and Lupton, R. H. and Schlegel, D. and Bahcall, N. A. and Brinkmann, J. and Brunner, R. J. and Budavári, T. and Csabai, I. and Castander, F. J. and Doi, M. and Fukugita, M. and Gyóry, Z. and Hamabe, M. and Hennessee, G. and Ichikawa, T. and Kunszt, P. Z. and Lamb, D. Q. and McKay, T. A. and Okamura, S. and Racusin, J. and Sekiguchi, M. and Schneider, D. P. and Shimasaku, K. and York, D., 2001, *AJ*, 122